Canards of mixed type in a neural burster

M. Desroches,[1,*] J. Burke,[2] T. J. Kaper,[2] and M. A. Kramer[2]

[1]*Department of Engineering Mathematics, University of Bristol, Bristol, United Kingdom*
[2]*Department of Mathematics and Statistics, Center for BioDynamics, Boston University, Boston, Massachusetts 02215, USA*

Canards are solutions of slow-fast systems that spend long times near branches of repelling equilibria, periodic orbits, or higher-dimensional invariant sets. Here, we report on the observation of a new type of canard orbit, labeled a canard of mixed type. This canard orbit is a hybrid of the classical limit cycle canards, which spend long times near attracting and repelling branches of equilibria, and torus canards, which spend long times near attracting and repelling branches of periodic orbits. The canards of mixed type arise in a model of neural bursting activity of fold-fold cycle type, and, as other canard phenomena, separate different dynamic states.

PACS number(s): 87.19.ll, 87.19.ln, 05.45.−a, 02.30.Oz

I. INTRODUCTION

The voltage activity of a single neuron generates many different types of dynamic behavior, including intervals of quiescence, intervals of spiking (periodic action potential generation), and intervals of bursting (spiking and quiescence interspersed) [1–3]. The dynamical mechanisms of these states have been studied extensively both experimentally and theoretically, including through mathematical modeling [4–7]. By contrast, the dynamical mechanisms governing the transitions between these states are not yet as well understood, and this subject is an active area of research. There exist a number of known transition scenarios. For example, between spiking and bursting the transition dynamics can include a blue sky catastrophe [8], period doubling [9], chaos [10,11], mixed-mode oscillations (MMOs) [12], or torus canards [13–15]. Here, we examine the transition between bursting and a fixed activity state, and show that this transition involves a new type of orbit which we call a *canard of mixed type* (CMT). In what follows, we first outline the general canard phenomenon for both planar and higher-dimensional systems. We then describe the model neural system, and examine the CMT through a slow-fast decomposition.

Canards are special, yet ubiquitous, solutions of differential equations with multiple time scales. The most well-studied canards are limit cycle canards. First encountered in the van der Pol model [16], limit cycle canards have been analyzed in one-parameter families of planar slow-fast vector fields [16–18] and arise in a diverse array of applications, ranging from neural and chemical models [19,20] to aircraft and laser dynamics [21,22]. These systems undergo Hopf bifurcations in which the attractor changes from a stable equilibrium to a stable relaxation oscillation; limit cycle canards occur exactly for parameter values in this transition. The limit cycle canard orbits consist of long time intervals spent, in alternation, near the attracting and repelling branches of equilibria of the fast system, obtained by freezing the slow dynamics and, hence, by considering the slow variable as a bifurcation parameter. Moreover, in bistable systems, the limit cycle canards come in two varieties: headless canards, which alternate between one attracting branch of equilibria and the repelling branch of equilibria, and canards with heads, which alternate between

both attracting branches and the repelling branch of equilibria [16]. These limit cycle canards also arise in higher-order models and are essential to understanding MMOs [23–26].

In higher-dimensional slow-fast systems, the canard phenomenon persists with enriched dynamics. When at least two fast variables are present, the fast system can display oscillatory dynamics and another form of canards is then possible, consisting of long segments near attracting and repelling *periodic orbits* in alternation. Such canards are referred to as *torus canards*. They have been observed in a five-dimensional model of a Purkinje cell [15] and have also been analyzed in a minimal three-dimensional system [13]. Moreover, torus canards occur in many well-known neural bursters, including in sub-Hopf–fold cycle bursting, circle-fold cycle bursting, and fold-fold cycle bursting [14]. In each of these neural models, torus canards appear during the transition between spiking and bursting activity and therefore are important for understanding the dynamical mechanisms of this transition [14]. Briefly, whether or not torus canards exist, or whether period doubling or other dynamics occur, depends on a number of factors, including the presence of attracting and repelling branches of slow manifolds, a torus bifurcation, and on local conditions of fold points on the slow manifolds. We refer the reader to Ref. [14], as well as to Refs. [8,12], for examples in which some conditions for torus canard existence are necessary or sufficient.

In general, canard orbits are solutions in slow-fast systems that follow attracting and repelling manifolds in the fast system, in alternation, as the slow system evolves. With this understanding, it becomes natural to expect additional types of canard orbits other than limit cycle canards and torus canards, corresponding to other types of connections between attracting and repelling manifolds of the fast system. The CMT orbits described in this paper are an example of this more general canard phenomenon, connecting a one-dimensional attracting manifold associated with equilibria in the fast system to a two-dimensional repelling manifold associated with limit cycles in the fast system. We find such canards in a simple model for interacting neural populations—an extended version of the Wilson-Cowan model [27]. The Wilson-Cowan model is a mean-field model representing the collective properties of large numbers of interacting neurons [28,29]. This model has served as a building block in a number of other models [30–33], in which the activity of each population modulates according to external inputs. We consider a modification of

*INRIA Paris-Rocquencourt Centre, Domaine de Voluceau - BP 105, 78153 Le Chesnay cedex, France.

the Wilson-Cowan model, utilized in Ref. [1], in which a slowly evolving variable modulates the excitability of the neural populations, and show that the canards of mixed type in this model separate regimes of bursting and fixed activity.

II. THE WILSON-COWAN-IZHIKEVICH (WCI) MODEL.

The WCI model, proposed by Izhikevich in Ref. [1], is a three-dimensional set of ordinary differential equations

$$\dot{x} = -x + S(r_x + ax - by + u), \tag{1a}$$

$$\dot{y} = -y + S(r_y + cx - dy + fu), \tag{1b}$$

$$\dot{u} = \varepsilon(k - x), \tag{1c}$$

where $S(x) = 1/[1 + \exp(-x)]$. With $0 < \varepsilon \ll 1$, the variables x and y are fast and u is slow. The WCI model can exhibit a wide variety of bursting dynamics, including fold-fold cycle bursting, where the active (i.e., rapid oscillation) phase of the burst initiates in a fold of fixed points and terminates in a fold of periodic orbits [1]. In Ref. [14] it was shown that, with the fixed parameters $r_y = -9.7$, $a = 10.5$, $b = 10$, $c = 10$, $d = -2$, $f = 0.3$, $\varepsilon = 0.03$, and for r_x in the range $-5.203 \leqslant r_x \leqslant -4.740$, the WCI model exhibits a transition from fold-fold cycle bursting to rapid spiking as k increases, and that this transition involves torus canards. Here we use the same values for the fixed parameters but consider larger values of r_x, in the range $-4.8 < r_x < -3$. We find in this case that the model exhibits a transition from fold-Hopf bursting to a state of fixed activity as k increases, and that this transition involves CMT. In what follows, all computations were performed using the software XPPAUT [34] and AUTO [35].

III. CANARDS OF MIXED TYPE IN THE WCI MODEL (1)

In this section, we give a detailed description of the CMT that appear in the WCI model and show how these dynamics arises naturally as one varies the parameter k. In addition, we analyze the saddle-focus equilibrium of the full system and identify its role in the creation of the CMT. Finally, we present a more complete two-parameter bifurcation analysis of the CMT in this model, and show that the CMT and torus canards exist in different parameter intervals.

A. Fundamental dynamics of CMT

Figure 1 shows an example of a CMT orbit at $(k,r_x) = (0.7752, -4.3)$. The time series of x, shown in Fig. 1(a), includes active ($x \sim 0.75$) and inactive ($x \sim 0$) phases of the orbit. The active phase includes three separate stages: an initial stage of active oscillations, followed by a stage of nearly fixed activity, followed by a second stage of active oscillations. To further describe this canard behavior, we consider a slow-fast decomposition of the system. First, we freeze the slow dynamics by setting $\varepsilon = 0$ in (1); in this way, u is treated as a bifurcation parameter in the fast system. The resulting bifurcation diagram [Fig. 1(b)] includes an S-shaped branch of fixed points which undergoes two saddle-node bifurcations (labels SNf, at $u \sim -1.8$ and $u \sim 1.1$) and three Hopf bifurcations (labels H, at $u \sim -1.6$, $u \sim 0.44$, and $u \sim 5.6$, though the third Hopf bifurcation is off scale in the figure). Two of these Hopf bifurcations are supercritical and

arranged so that periodic orbits born in one terminate in the other. The third Hopf bifurcation at negative u is subcritical with an associated branch of periodic orbits that terminates in a homoclinic bifurcation (label HC).

The bursting orbits of the full system [Fig. 1(b)] evolve through the bifurcation diagram of the fast system. The active phase of the burst initiates near the saddle-node of fixed points at $u \sim 1.1$ and terminates near the subcritical Hopf bifurcation at $u \sim -1.6$. The three stages of the active phase of the burst are labeled in the bifurcation diagram. During the first stage of active oscillations, the full system trajectory follows the attracting branch of limit cycles of the fast system. As u decreases the trajectory passes through the supercritical Hopf bifurcation of the fast system at $u \sim 0.44$ and follows the attracting branch of equilibria of the fast system; this corresponds to the stage of nearly fixed activity. As the slow variable u decreases further, the orbit of the full system approaches the subcritical Hopf bifurcation of the fast system at $u \sim -1.6$. During the second stage of active oscillations, the trajectory follows the repelling branch of limit cycles of the fast system, with u reversing direction and slowly increasing [Fig. 1(c)]; the evolution of the slow variable u during the CMT orbit can be understood by considering the average $\langle x \rangle$—see Ref. [8]. During the time interval when the canard is near the branch of attracting equilibria, the average $\langle x \rangle$ is greater than $k = 0.7752$ and the slow drift is in the direction of decreasing u. In contrast, during the time interval when the canard is near the branch of repelling periodic orbits, $\langle x \rangle$ is less than 0.7752 and u increases slowly. The second stage of active oscillations ends when the trajectory returns to the lower branch of attracting fixed points of the fast system, corresponding to the inactive phase of the burst.

We conclude that, during the burst's active phase, the full system dynamics involves a combination of attracting limit cycles, attracting fixed points, and repelling periodic orbits in the fast system. By definition, this corresponds to a canard behavior and, to our knowledge, this form of canard trajectory (CMT) has not been previously reported.

B. The second stage of active oscillations and its trigger

In the previous section we described the CMT phenomenon for a fixed value of k. We now describe the model dynamics for a range of k and show that the CMT separates the bursting and fixed regimes of the neural dynamics.

For $k \leqslant 0.7$, the system displays the standard fold-Hopf type bursting [1]. That is, the full system attractor exhibits an active phase of rapid oscillations that begins in a fold of fixed points of the fast system and ends in a Hopf bifurcation in the fast system. For slightly larger values of $k \in [0.7, 0.722]$, the saddle equilibrium in the full system starts affecting the shape of the bursting attractor. In the classic fold-Hopf bursting (for $k \leqslant 0.7$), when the active burst stage ends, the orbit escapes in the (vertical) direction of the fast fibers. But, for $k \in [0.7, 0.722]$, the unstable manifold of the saddle equilibrium in the full system affects the direction of the orbit escape, causing a subtle bend in the near-vertical descent [Figs. 2(a1)–2(b1), where $k = 0.72$ and the inset panel]. The impact of this saddle equilibrium in the full system on the transition from fold-Hopf bursting is further discussed in Sec. III C.
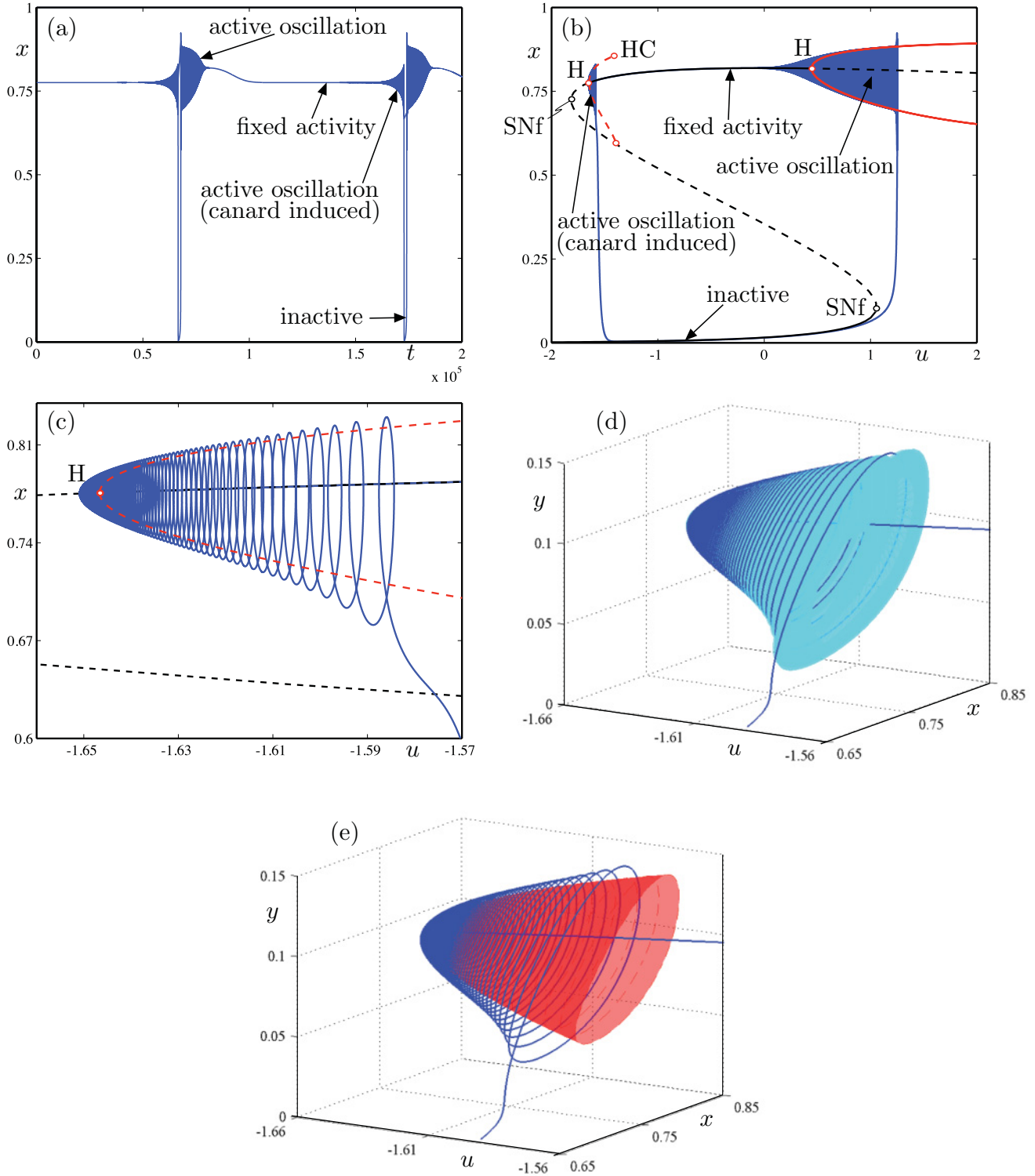
FIG. 1. (Color online) Canard of mixed type in the WCI model (1) at $(k, r_x) = (0.7752, -4.3)$. (a) shows the time series for variable x of the canard of mixed type trajectory. The labels indicate the inactive phase of the burst, as well as the three different stages of the active phase of the burst. (b) shows the same trajectory (blue or gray) in the phase plane (u, x) together with the bifurcation diagram of the fast system. The black curves indicate branches of stable (solid) or unstable (dashed) fixed points, and the red (gray) curves indicate the extrema of stable (solid) or unstable (dashed) limit cycles. Note that the bifurcation diagram of the fast system for (b) is valid for any value of k. (c) is an enlargement of (b) showing the second stage of active oscillations, where the canard orbit in the full system is observed to spend a long time near the family of repelling periodic orbits (a two-dimensional surface, shown here at the extrema in x) in the fast system. (d) shows a three-dimensional view of the canard orbit in the phase space (x, y, u) together with the two-dimensional unstable manifold (light-shaded surface) of the saddle-focus equilibrium that exists for this parameter value. Finally, (e) shows the same orbit together with the u-dependent family of repelling limit cycles of the fast system (surface). Note that the surface on (d) lies outside that shown in (e).
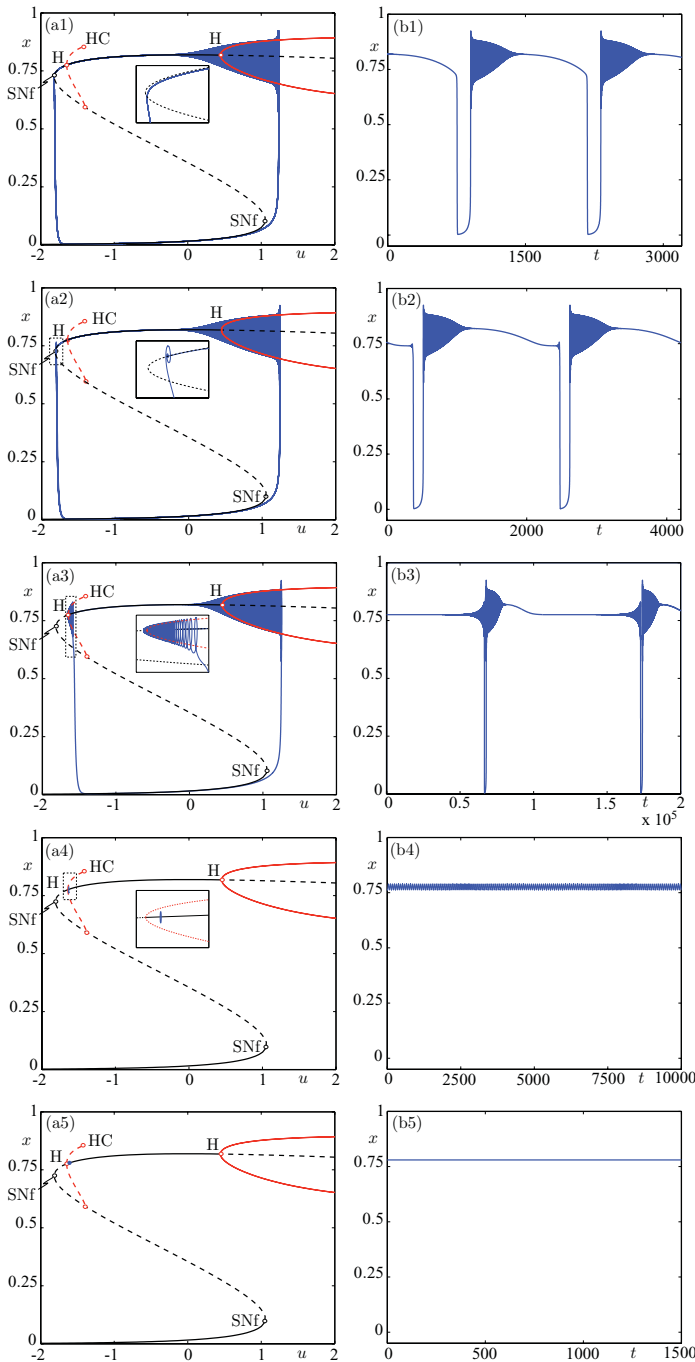
FIG. 2. (Color online) Dynamical transition in the WCI model from fold-Hopf bursting [(a1)–(b1), $k = 0.72$] to a stable equilibrium via fold-Hopf bursting with additional (small-amplitude) fast oscillations close to a saddle-focus equilibrium [(a2)–(b2), $k = 0.74$], the canard of mixed type regime [(a3)–(b3), $k = 0.7752$], small-scale oscillations [(a4)–(b4), $k = 0.776$], and fixed activation [(a5)–(b5), $k = 0.78$]. Labels and curves as in Fig. 1. Note that (a3) is identical to Fig. 1(b).

For $0.722 \leqslant k \leqslant 0.775287$, the bursting profile of the full system attractor remains qualitatively similar to the fold-Hopf bursting observed at smaller values of k. However, a second epoch of fast oscillations within each burst period emerges, resulting from a saddle-focus equilibrium point in the full system. This "second active stage" within each burst appears just before the return to the quiescent burst stage [Figs. 2(a2)–2(b2), where $k = 0.74$]. Therefore, this type of bursting can effectively be described as fold-Hopf bursting "augmented" by a second oscillatory stage that is entirely due to the saddle focus in the full system. Initially, the duration of this second active stage does not vary upon an increase of k, only its position in the u-x phase space shifts to larger values of u, following the

movement of the saddle-focus equilibrium of the full system; see Fig. 2(a2), inset panel.

Further increases in k result in a large increase in the amplitude of the second active stage of the burst. This dramatic increase corresponds to the emergence of the CMT, in which the full system dynamics follow the branch of repelling limit cycles of the fast system [Figs. 2 (a3)–2(b3), where $k = 0.7752$]. The interval of parameter values in which the CMT exist is approximately $k \in [0.7752, 0.77528]$.

At a value of k slightly larger than $k \sim 0.77528$, the full system undergoes a torus bifurcation, resulting in weakly damped quasiperiodic oscillations that mark the end of the CMT regime and correspond to the solutions of system (1)

displaying weakly damped quasiperiodic oscillations. Increasing k further ends the bursting dynamics of the full system. The attractor of the full system becomes a stable limit cycle toward which the full system converges after some weakly damped quasiperiodic oscillations [Figs. 2(a4)–2(b4), where $k = 0.776$]. Stable limit cycles persist until k increases beyond the supercritical Hopf bifurcation that generates this branch of stable limit cycles in the full system, at $k \sim 0.77665$. Further increases in k past this value cause the full system's trajectory to converge toward a stable equilibrium; see Figs. 2(a5)–2(b5), where $k = 0.78$. This stable equilibrium is located on the upper branch of the curve of equilibria of the fast system and marks the end of the bursting regime. Biophysically, we may interpret these dynamics as a persistent activity state without modulations.

We conclude that the CMT regime occurs within the transition between the bursting and fixed activity regimes as k increases in this model. In the next section we examine this dynamical transition through the CMT regime from the viewpoint of the invariant manifolds of the saddle-focus equilibrium of the full system.

C. The roles of the saddle-focus equilibrium in the full system and its invariant manifolds in CMT

CMT can be further understood by examining the stable and unstable manifolds of the saddle-focus equilibrium that exists in the full system. This saddle-focus equilibrium has a one-dimensional stable manifold that approaches it close to the attracting branch of equilibria of the fast system—that exists between the subcritical and supercritical Hopf bifurcations in Fig. 1(b)—and a two-dimensional unstable manifold that has locally the shape of a paraboloid [Fig. 1(d)] and is close to the family of repelling cycles of the fast system [Fig. 1(e)]. We computed this two-dimensional unstable manifold by continuation of a family of orbit segments whose initial conditions lie on a circle of small radius in the unstable eigenspace of the equilibrium; for more details about such computations, see, e.g., Ref. [36]. Hence, the CMT trajectory follows successively both invariant manifolds of the saddle-focus equilibrium in the full system.

As observed in other canard phenomena, the CMT appear only in a narrow range of parameter values. For k greater than approximately 0.722, the equilibrium of the full system, located close to the upper fold of fixed points shown in Fig. 1(b), has complex eigenvalues. Consequently, the bursting attractor of system (1) leaves the vicinity of the upper branch of equilibria of the fast system by spiralling out along the two-dimensional unstable manifold of this saddle focus. However, such a bursting orbit does not correspond to a CMT yet. Indeed, the saddle-focus equilibrium of the full system is located sufficiently far from the subcritical Hopf bifurcation point of the fast system such that the fast spiralling motion is not close to the envelope of the repelling orbits in the fast system. Increasing k to 0.7752 brings the saddle-focus equilibrium close enough to the subcritical Hopf bifurcation so that this fast spiraling motion stays close to the family of repelling cycles, hence giving a canard segment. From this moment on, the evolution of the CMT is explosive and the canard segment gets longer until, at $k \sim 0.775\,287$, the global

bursting dynamics is destroyed. For this value of k and slightly higher values as well, any trajectory with initial conditions close to the upper attracting branch of equilibria of the fast system displays weakly damped quasiperiodic oscillations which, after a transient has passed, eventually converge to a stable equilibrium. Hence, it is useful to study the full system's bifurcations and invariant manifolds in order to better understand the dynamics of CMT.

The saddle equilibrium in the full system also affects the dynamics of the fold-Hopf bursting. In particular, the shape of its strong unstable manifold changes upon variation of k and dictates how the periodic orbit behaves near the saddle equilibrium and evolves from fold-Hopf bursting to the CMT regime. A more thorough investigation of the role of the strong stable manifold in this transition will be considered in future work.

D. The locus of CMT in the (u, r_x) parameter space

To explore how the dynamics also depend on parameter r_x, we consider the bifurcations of the fast system in the two-parameter plane (u, r_x). In this plane different types of canard behaviors can be encountered; see Fig. 3. Several branches of codimension-one bifurcations are highlighted, in particular, loci of Hopf bifurcation points (H), of saddle nodes of equilibria (SNf), of saddle nodes of periodic orbits (SNp), and of homoclinic points (HC). Along these branches, codimension-two points (circles) play the role of organizing centers for the dynamics of the full system. In particular, the Bautin point (B) corresponds to a transition from supercritical Hopf bifurcation to subcritical Hopf bifurcation, and also to the end of the SNp branch. In this model, the Bautin bifurcation separates the region where torus canards are expected from the region where CMT can occur. Torus canards require a fold of periodic orbits [14], while the CMT described here require a
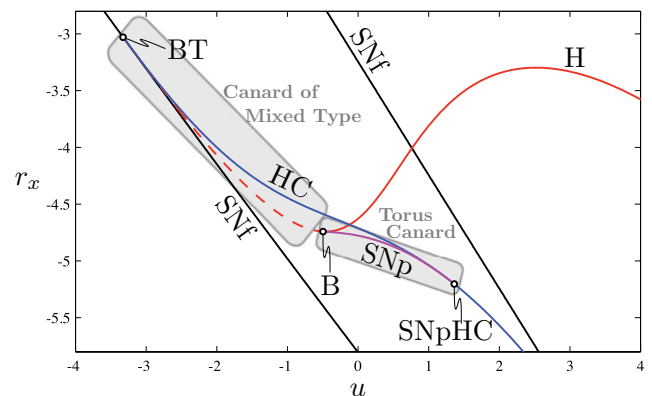
FIG. 3. (Color online) Two-parameter bifurcation diagram of the fast system of the WCI model in the (u, r_x) plane. Several branches are shown, corresponding to loci of codimension-one bifurcations; these include supercritical Hopf bifurcations (H, solid curve), subcritical Hopf bifurcations (H, dashed curve), saddle node of fixed points (SNf), and homoclinic bifurcations (HC). Codimension-two points organize the dynamics; these include a Bautin point (B), a Bogdanov-Takens point (BT), and a point where a saddle node of periodic orbits collides with a homoclinic bifurcation (SNpHC). The regions of this parameter plane where torus canards and CMT are expected to occur are labeled and highlighted by gray boxes.

subcritical Hopf bifurcation. We therefore conclude that this model exhibits two types of canard behavior—torus canards and CMT—both of which occur at the transitions from bursting to another type of activity.

IV. CONCLUSION

In this paper, we presented a new form of canard dynamics, the canards of mixed type (CMT), in the context of a neural burster, the Wilson-Cowan-Izhikevich (WCI) model. Such orbits follow successively a branch of attracting equilibria and a branch of repelling limit cycles of the fast system. In this particular model, CMT organize the transition from bursting to a regime of fixed activity in the neuron. In the CMT regime, the bursting attractor of the system develops another active rapid oscillation corresponding to the orbit spiraling on the fast time scale close to the repelling cycles of the fast dynamics. This new type of bursting dynamics is reminiscent of another

form of canards, the torus canards, which can be related to the transition from bursting to spiking regimes; in particular, torus canards can also be found in the WCI model but for a different set of parameters. Finally, we note that this new form of canard dynamics arises due to a relatively commonly occurring configuration in terms of bifurcations of the fast system and, hence, can be expected to occur in a large class of neural bursters.

[1] E. M. Izhikevich Int. J. Bifurcation Chaos Appl. Sci. Eng. **10**, 1171 (2000).

[2] J. Rinzel, in *Mathematical Topics in Population Biology, Morphogenesis, and Neurosciences*, edited by E. Teramoto and M. Yamaguti, Lecture Notes in Biomathematics Vol. 71 (Springer, Berlin, 1987).

[3] J. L. Hindmarsh and R. M. Rose, Proc. R. Soc. London B **221**, 87 (1984).

[4] E. M. Izhikevich, SIAM J. Appl. Math. **60**, 503 (1999).

[5] L. G. Nowak, M. V. Sanchez-Vives, and D. A. McCormick, Cereb. Cortex **7**, 487 (1997).

[6] J. Rinzel and G. B. Ermentrout, in *Methods in Neural Modeling. From Synapses to Networks*, edited by C. Koch and I. Segar (MIT Press, Cambridge, MA, 1989), pp. 135–169.

[7] D. Terman, SIAM J. Appl. Math. **51**, 1418 (1991).

[8] A. Shilnikov and G. Cymbalyuk, Phys. Rev. Lett. **94**, 048101 (2005).

[9] G. Cymbalyuk and A. Shilnikov, J. Comput. Neurosci. **18**, 255 (2005).

[10] G. S. Medvedev, Phys. Rev. Lett. **97**, 048102 (2006).

[11] D. Terman, J. Nonlin. Sci. **2**, 135 (1992).

[12] J. Wojcik and A. Shilnikov, Physica D **240**, 1164 (2011).

[13] G. N. Benes, A. M. Barry, T. J. Kaper, M. A. Kramer, and J. Burke, Chaos **21**, 023131 (2011).

[14] J. Burke, M. Desroches, A. M. Barry, T. J. Kaper, and M. A. Kramer, J. Math. Neurosci., 2012 (in press).

[15] M. A. Kramer, R. D. Traub, and N. J. Kopell, Phys. Rev. Lett. **101**, 068103 (2008).

[16] E. Benoît, J.-L. Callot, F. Diener, and M. Diener, Collect. Math. **32**, 37 (1981).

[17] W. Eckhaus, in *Asymptotic Analysis II*, edited by F. Verhulst, Lecture Notes in Mathematics Vol. 985 (Springer, Berlin, 1983), pp. 449–494.

[18] M. Krupa and P. Szmolyan, J. Differ. Equations **174**, 312 (2001).

[19] M. Brøns and K. Bar-Eli, J. Phys. Chem. **95**, 8706 (1991).

[20] J. Moehlis, J. Math. Biol. **52**, 141 (2006).

[21] M. Brøns, Math. Eng. Industry **2**, 51 (1988).

[22] V. Z. Tronciu, H.-J. A. Wunsche, K. R. Schneider, and M. Radzuinas, Proc. SPIE **4283**, 347 (2001).

[23] M. Krupa, N. Popović, N. Kopell, and H. G. Rotstein, Chaos **18**, 5106 (2008).

[24] N. Popović, J. Phys.: Conf. Ser. **138**, 012020 (2008).

[25] H. G. Rotstein, M. Wechselberger, and N. Kopell, SIAM J. Appl. Dyn. Syst. **7**, 1582 (2008).

[26] T. Vo, R. Bertram, J. Tabak, and M. Wechselberger, J. Comput. Neurosci. **28**, 443 (2010).

[27] H. R. Wilson and J. D. Cowan, Biophys. J. **12**, 1 (1972).

[28] A. Destexhe and T. J. Sejnowski, Biol. Cybern. **101**, 1 (2009).

[29] S. Coombes, Neuroimage **52**, 731 (2010).

[30] S. Coombes, B. Doiron, K. Josić, and E. Shea-Brown, Philos. Trans. R. Soc., A **364**, 3301 (2006).

[31] R. F. Galán, PLoS ONE **3**, e2148 (2008).

[32] S. J. Schiff and T. Sauer, J. Neural. Eng. **5**, 1 (2008).

[33] G. Deco, V. Jirsa, A. R. McIntosh, O. Sporns, and R. Kötter, Proc. Natl. Acad. Sci. USA **106**, 10302 (2009).

[34] G. B. Ermentrout, *Simulating, Analyzing, and Animating Dynamical Systems: A Guide to XPPAUT for Researchers and Students* (SIAM, Philadelphia, 2002).

[35] E. J. Doedel, A. R. Champneys, T. Fairgrive, Yu. Kuznetsov, B. Oldeman, R. Paffenroth, B. Sandstede, X. Wang, and C. Zhang, *AUTO-07P: Continuation and Bifurcation Software for Ordinary Differential Equations*, available at [http://indy.cs.concordia.ca/auto].

[36] B. Krauskopf, H. M. Osinga, E. J. Doedel, M. E. Henderson, J. Guckenheimer, A. Vladimirsky, M. Dellnitz, and O. Junge, Int. J. Bifurcation Chaos Appl. Sci. Eng. **15**, 763 (2005).